École Polytechnique Fédérale de Lausanne

Towards replicating the full chewing process : Initial development of a Stewart platform-based chewing robot.

Master thesis

Author :

Barbara De Groot, 296815

CREATE Lab, Prof. Josie Hughes
Supervisor : Benhui Dai

June 12, 2025

Contents

1 Introduction **2**

2 Methods **3**

2.1 Design requirements from human physiology 3

2.2 Mechanical design 3

2.3 Control 7

2.3.1 Hardware (electronics) 7

2.3.2 Software architecture 8

2.3.3 Stewart platform control 9

2.4 Data acquisition and processing 10

3 Results **11**

3.1 Mimicking human jaw motion 11

3.2 chewing force 11

4 Discussion **11**

4.1 Summary of findings 11

4.2 Limitations 11

4.3 Future work 12

5 Conclusion **12**

6 References **13**

1 Introduction

Human chewing is a complex process, involving different systems such as the jaw, teeth, tongue and saliva, all coordinated to break down food into a bolus that can be swallowed and digested. Chewing robots are a great tool to study this process that is not yet fully understood as they give us the opportunity for a closely controlled environment where each parameter can be adjusted and measured. This makes them valuable not only for advancing our understanding of chewing mechanics and related disorders, but also for a wide range of applications. In dentistry, they are used to test how implants and other dental devices wear over time. In food science, they help assess texture and flavor release during mastication. They also offer a reliable platform for studying the release of active compounds in chewable medications such as medical chewing gum.

Nowadays, many mastication robots exist, and while most are limited in their ability to fully mimic human chewing due to restricted degrees of freedom, some have already made significant progress. For example, the Bristol Dento-Munch Robo-Simulator [1] features 6 degrees of freedom (DoF), closed-loop control, force feedback, and a full set of teeth capable of replicating human chewing forces. Similarly, the robot developed by Seung-Ju Lee [2] offers the same capabilities, with a design that more closely follows human biomechanics. Another system, by Alemzadeh et al. [3], includes a closed mouth and artificial saliva—two important components of realistic mastication—even though it has limited sensory feedback. However, no existing system combines all critical elements: 6 DoF, position and multidirectional force feedback, a hermetically closed mouth with saliva circulation, and an actuated tongue. The absence of the tongue is particularly important, as it directs food toward the molars and mixes it with saliva during chewing.

This project addresses that gap by taking the first step toward an all-inclusive chewing robot. Because only four months were available and no previous hardware existed, the present work concentrates on the mechanical foundation: a modular 6-DoF Stewart platform-based jaw sized from physiological data, equipped with tri-axial force sensing and position feedback. The overarching research question is therefore narrowed to:

How can a modular Stewart-platform jaw be designed and validated so that it reproduces human chewing trajectories and forces while exposing interfaces for future tongue and saliva modules?

To answer this question, we (i) designed and built the platform, (ii) implemented a simple closed-loop control system that can be scaled in later iterations, (iii) recorded our own motion-capture dataset of human chewing, and (iv) replayed these trajectories on the robot to assess its performance. By laying down a flexible, expandable foundation, this work enables future integration of artificial saliva flow, an artificial tongue and adaptive bio-inspired control, moving one step closer to a robot that replicates the complete human chewing process.

2 Methods

2.1 Design requirements from human physiology

The jaw makes essential contributions to the chewing process such as generating the forces required to break down food, controlling the lower mandible motion and giving sensory feedback. A robotic jaw should therefore be able to mimic these functions as closely as possible. As this is the first iteration of the chewing robot, we focus on force generation and range of motion, while sensory feedback and other functions can be added in future iterations. The design requirements are based on the literature and the human jaw anatomy and physiology, as summarized in Table 1. Note that the jaw's speed is not a design requirement as food can be effectively chewed even at slow speeds.

Quantity	**Values reported in the literature**	**Design requirement**
Degrees of freedom (DoF)	6 DoF: 3 translational (X, Y, Z) and 3 rotational (roll, pitch, yaw) [4]	6 DoF
Vertical (compressive) bite force F_z	600 N chewing force in healthy adults [5], 1243 N maximum clenching force [6]	800 N
Lateral force F_x	-72 N (left) to $+53$ N (right) during maximal biting [7]	± 100 N
Anterior–posterior force F_y	-10 N (posterior) to $+30$ N (anterior) [7]	± 50 N
Mandibular motion range	14 mm lateral shift, 11 mm protrusion, 61 mm mouth opening in healthy adults [8]	± 20 mm (X, Y); 0–70 mm (Z)

Table 1: Functional design requirements.

2.2 Mechanical design

The first major design decision was how to achieve 6 degrees of freedom (DoF) for jaw motion. In the field of robotic mastication, two common approaches are used. The first is a biomechanically inspired design using linear actuators [2] or combinations of actuated cables and springs [3] to replicate muscle behavior. The second is a Stewart platform [1]—a widely used 6-DoF parallel mechanism, often seen in motion simulators. See Figure 1 for a visualization of the two approaches.

For this project, we chose the Stewart platform approach. Its well-defined kinematics and ease of control make it particularly suitable for our goal of replicating recorded human chewing motion. Because our control strategy is based on reproducing real motion trajectories, having a platform with straightforward inverse kinematics is a key advantage.

Stewart platforms generally come in two configurations: one based on rotary servo motors and one based on linear actuators, see Figure 1. We selected the linear actuator design for several reasons. It offers more efficient force transmission, a simpler kinematic model, and greater structural rigidity—all important factors when attempting to reproduce the forces involved in human chewing.

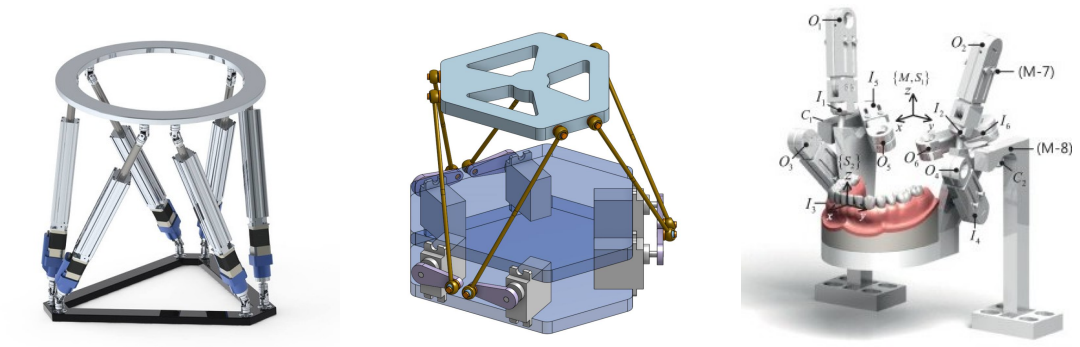

(a) **(b)** **(c)**

Figure 1: (a) Linear actuator-based jaw design. (b) Rotary servo motor-based Stewart platform. (c) Biomechanically inspired design[2].

The platform's dimensions were determined based on actuator specifications, desired jaw range of motion, and the working space required. The working space refers to the overall range of jaw motion and is defined by functional requirements summarized in Table 1. Based on findings in [9], we prioritized achieving the necessary vertical range of motion, knowing that sufficient horizontal range would follow.

Assuming a minimum actuator mounting angle of 45° to the horizontal, the minimum required stroke length is calculated as:

$$l_{\min} = \frac{z_{\max} - z_{\min}}{\sin(45°)} = \frac{70\,\text{mm}}{\sin(45°)} \approx 99\,\text{mm} \tag{1}$$

To meet the minimum vertical force requirement of 800 N, each actuator must provide:

$$F_{\min} = \frac{F_{z,\min}}{6 \cdot \sin(45°)} = \frac{800\,\text{N}}{6 \cdot \sin(45°)} \approx 189\,\text{N} \tag{2}$$

With this minimum actuator force, we estimate the lateral (shear) and front-back force capacities as:

$$F_x \approx 2 \cdot \cos(45°) \cdot F_{\min} + 4 \cdot \cos(45°) \cdot \sin(30°) \cdot F_{\min} \approx 534\,\text{N} \gg 100\,\text{N} \tag{3}$$

$$F_y \approx 4 \cdot \cos(45°) \cdot \cos(30°) \cdot F_{\min} \approx 462\,\text{N} \gg 50\,\text{N} \tag{4}$$

These calculations show that ensuring the vertical force requirement is met also guarantees that shear forces in the x and y directions will exceed their respective targets.

Since speed is not a strict requirement for this prototype, we prioritized force over velocity when selecting actuators. Position feedback is necessary for closed-loop control, as we use inverse kinematics to compute actuator positions based on the desired platform pose.

We selected the PA-14P-4-50 linear actuator, which meets both stroke and force requirements as seen in Table 2. The dimensions of both base and platform, see Figure 2, were chosen to accomodate the size of the actuators. The resulting vertical workspace of the platform is 118 mm, which is more than enough to cover the required 70 mm.

Parameter	Value
Stroke length	101 mm
Max force	222.4 N
Speed (no load)	28 mm/s
Speed (full load)	21 mm/s
Position feedback	Potentiometer
Protection class	IP54
Power supply	12 V DC

Table 2: PA-14P-4-50 specifications.

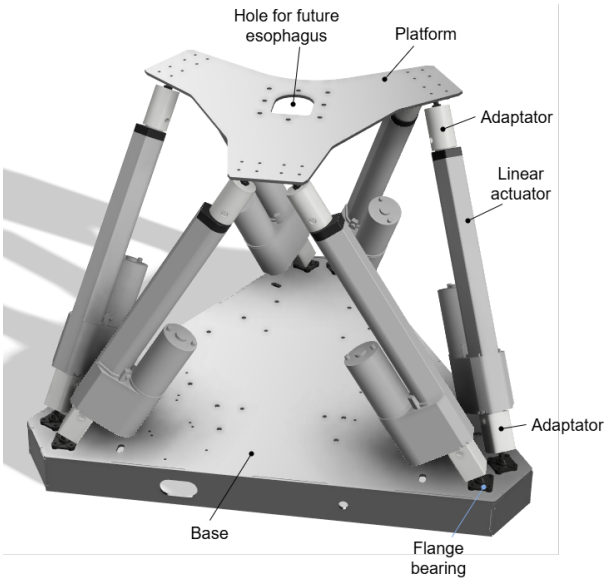

Figure 2: Final stewart platform design.

Next, we designed the upper and lower jaws, which are attached to the platform and base respectively. The lower jaw is mounted on the moving platform and elevated using four aluminum rods. This elevation provides two main advantages: it creates a clear line of sight to place a motion capture marker on the gnathion, and it leaves space beneath the jaw for integrating a future esophagus module. The mandibular teeth are fixed to a rigid plate and positioned slightly forward to leave room for a future tongue module. See Figure 3a.

The upper jaw is mounted on a rigid frame made of aluminum rods to ensure sufficient stability and stiffness under loading. This rigidity is essential to resist the forces applied by the lower jaw during chewing. Three-axis load cells are installed on the upper jaw mounting plate to measure both vertical and lateral forces during contact. Two acrylic adaptor plates connect these load cells to the maxillary teeth. Each adaptor has a central opening reserved for a future camera, which will be used to observe food behavior during mastication. See Figure 3b.

Both the maxillary and mandibular teeth are designed to be easily replaceable through the use of acrylic adaptor plates. This modularity allows for testing different tooth shapes, materials, and conditions (e.g., healthy, aged, or damaged teeth), which will be important for future studies on chewing development and masticatory disorders.

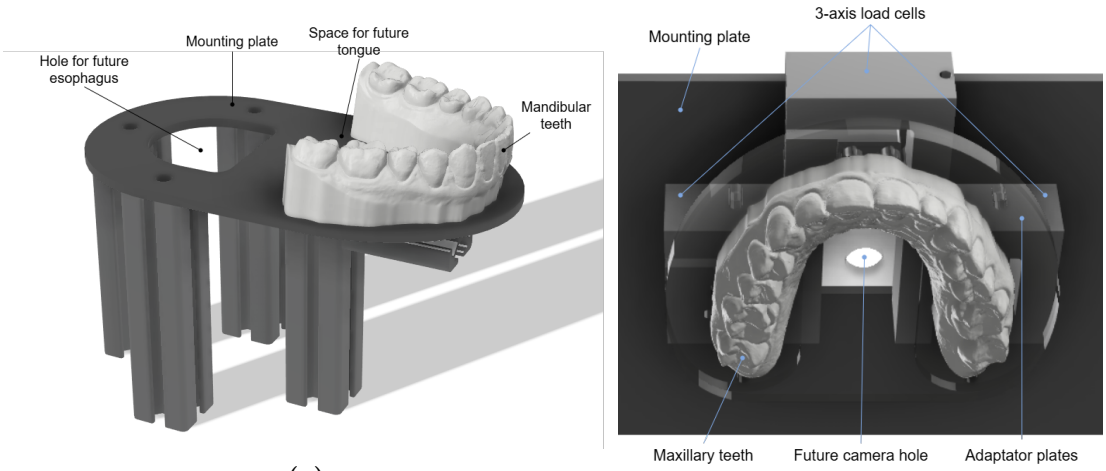

(a) **(b)**

Figure 3: (a) Annotated lower jaw design. (b) Annotated upper jaw design.

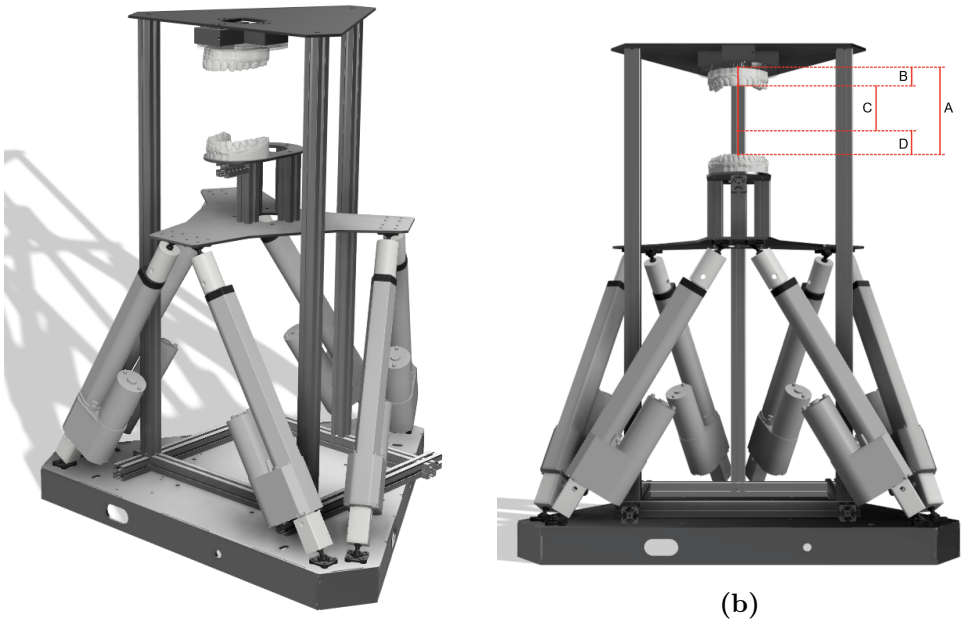

(a) **(b)**

Figure 4: (a) Final design overview. (b) Workspace design: A-Full vertical workspace of 118mm; B-Upper margin of 25mm; C-Working chewing volume of 60mm; D-Bottom margin of 33mm.

The final design is shown in Figure 4a. The height of the upper jaw subsystem was set slightly below the platform's maximum vertical reach—roughly centered in the middle of its vertical workspace. This positioning ensures that the robot can apply maximum vertical force when the mandibular and maxillary teeth are in contact, while still allowing enough range to meet angular requirements during chewing. A detailed view of the vertical workspace can be found in Figure 4b.

The base, platform, lower jaw mount, and upper jaw mount are all made out of steel, see Table 3. Although heavier than aluminum, steel offers significantly higher stiffness, with a Young's modulus of 190-210 GPa. This makes it a better choice for components that require

high rigidity and minimal deformation under load. Additionally, steel's weldability makes it practical for future modifications—for example, adding reinforcement ribs to the upper jaw mounting plate to further improve structural stability.

Subsystem	Part	Material
Stewart Platform	Base	Steel
	Platform	Steel
	Adaptator	PLA
Lower Jaw	Lower jaw mounting plate	Steel
	Mandibular teeth	PLA
Upper Jaw	Upper jaw mounting plate	Steel
	Upper jaw adaptator plates	Acrylic
	Maxillary teeth	PLA

Table 3: Mechanical design materials.

Waterproofing. As the robot is designed to eventually include a saliva module, it is important to ensure that the electronics and mechanical components are protected from moisture. First, we protected the steel parts with a layer of paint to prevent rusting. Then on both the upper and bottom side of the base, a plastic sheet was added to cover the electronics and prevent water from entering inside the box and damaging the electronics. Finally, the linear actuators are IP54 rated, meaning they are protected against dust and splashes of water from any direction.

2.3 Control

2.3.1 Hardware (electronics)

A Teensy 4.1 (600 MHz ARM Cortex-M7, single-precision FPU) executes the control loop.Its key peripherals are:

- three 12 A dual DC motor drivers (DF Robot) controlling the six linear actuators;
- six analogue inputs reading potentiometer position feedback from the linear actuators;
- three transmitters for the load cells mounted on top of the maxilla;
- an on-board micro-SD slot used for trajectory files and calibration data.

A 12 V AC/DC brick powers the actuators directly; the user's computer supplies 5 V to the Teensy, which in turn sources the 3.3 V logic rails for the motor drivers and load-cell transmitters. The full electronics schematic is shown in Fig. 5.

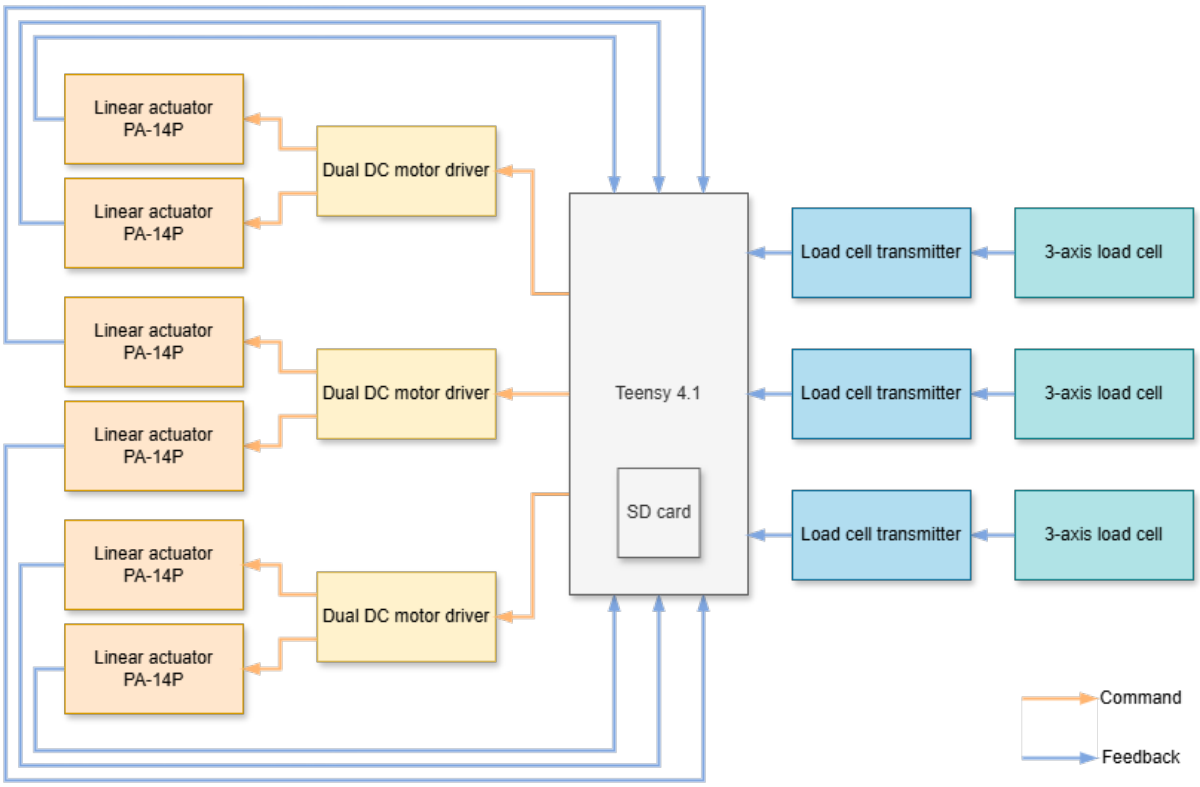

Figure 5: Electronics schematic.

2.3.2 Software architecture

The central class `RobotController` maintains the finite-state machine in Fig. 7 and manages two modules:

- `StewartPlatform`: inverse kinematics, trajectory interpolation, and low-level actuator commands;
- `ForceSensing`: continuous load-cell acquisition and filtering;

The controller is designed to be modular, allowing for easy addition of new modules such as a tongue or saliva module in the future. The three controller states are:

1. **Stop** – return to home pose; reload trajectory if the user selects a new file;
2. **Calibrate** – user can manually change the initial (x, y, z) position via the GUI;
3. **Move** – replay the selected trajectory.

A lightweight Python GUI on the host PC issues high-level commands, such as state changes, and plots sensor data.

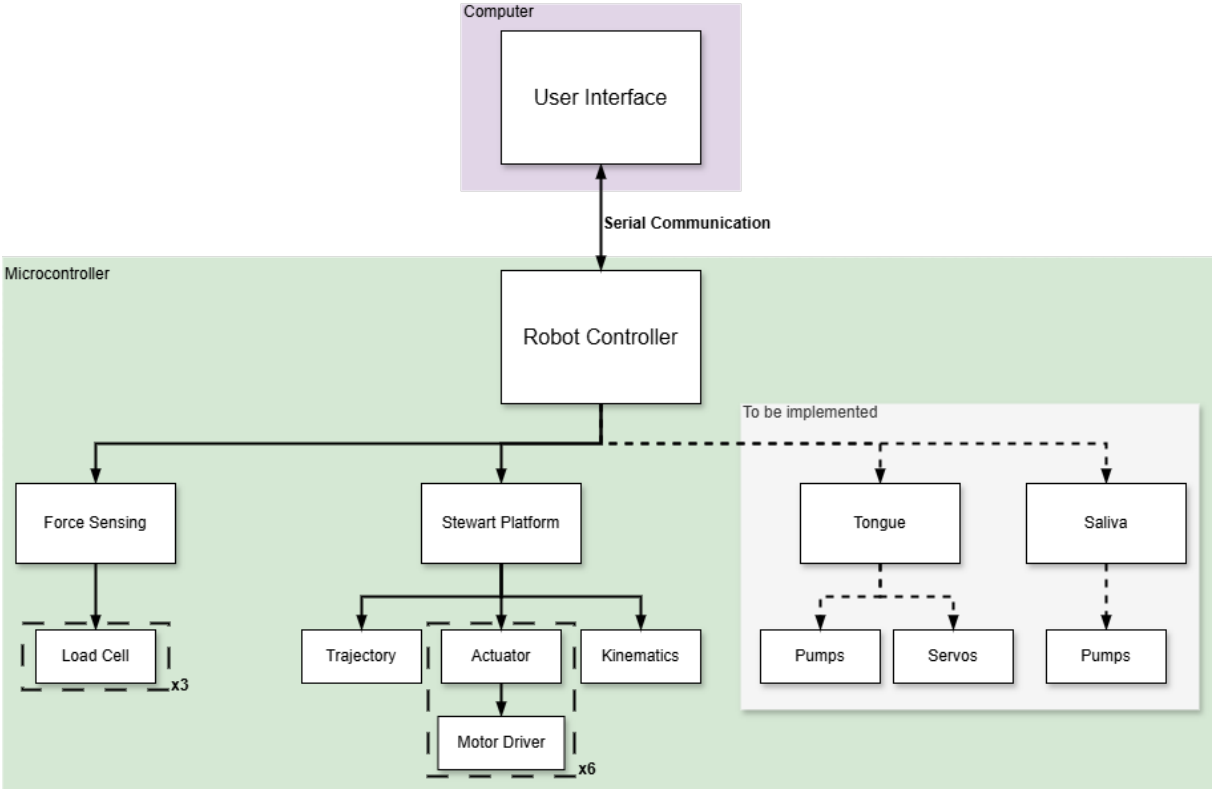

Figure 6: Overall code structure.

Figure 7: Robot controller state machine.

2.3.3 Stewart platform control

The Stewart platform is controlled by the `StewartPlatform` class, which implements the following functionalities:

Trajectory interpolation The Stewart Platform follows a 3D trajectory (x, y, z, roll, pitch, yaw) from a .csv file on the micro-SD card. See section 2.4 for details on the recording protocol and data processing. Each pose is defined by its position $\mathbf{t} = (x, y, z)$ and orientation given by the Euler angles (ϕ, θ, ψ), which are the roll, pitch, and yaw angles respectively. The trajectory is then linearly interpolated with a fixed time step chosen by the user.

Inverse kinematics For each pose in the trajectory, `Kinematics` computes the lengths of the six linear actuators that will achieve the desired pose of the platform, i.e. the inverse kinematics. To do so, we first compute the standard rotation matrix $R(\phi, \theta, \psi)$ for the Euler angles, which is defined as the product of three rotation matrices about the Z, Y, and X axes:

$$R(\phi,\theta,\psi) = R_Z(\psi)R_Y(\theta)R_X(\phi) = \begin{pmatrix} \cos\psi & -\sin\psi & 0 \\ \sin\psi & \cos\psi & 0 \\ 0 & 0 & 1 \end{pmatrix} \begin{pmatrix} \cos\theta & 0 & \sin\theta \\ 0 & 1 & 0 \\ -\sin\theta & 0 & \cos\theta \end{pmatrix} \begin{pmatrix} 1 & 0 & 0 \\ 0 & \cos\phi & -\sin\phi \\ 0 & \sin\phi & \cos\phi \end{pmatrix}$$

The platform joints $\mathbf{p}_i$, i being the actuator index, are then rotated about a fixed point $\mathbf{c}$, which is the front of the gnathion, and translated by the user-defined home position $\mathbf{t} = (x, y, z)$, resulting in the world coordinates of the platform joints:

$$\mathbf{w}_i = R(\mathbf{p}_i - \mathbf{c}) + \mathbf{c} + \mathbf{t}.$$

Finally, the actuator length is the Euclidean distance to the fixed base joint $\mathbf{b}_i$:

$$\ell_i = \|\mathbf{w}_i - \mathbf{b}_i\|_2.$$

PI controller For each actuator, its desired length is sent to a PI position controller, see Figure 8. The PI gain values are set to $K_P = 25$ and $K_I = 0.1$, which were determined empirically to achieve a good trade-off between responsiveness and stability. An anti-windup mechanism is implemented to prevent the integral term from growing too large, which could lead to overshooting. To minimize the noise of the potentiometer feedback, we apply a low-pass filter averaging the last 10 samples.

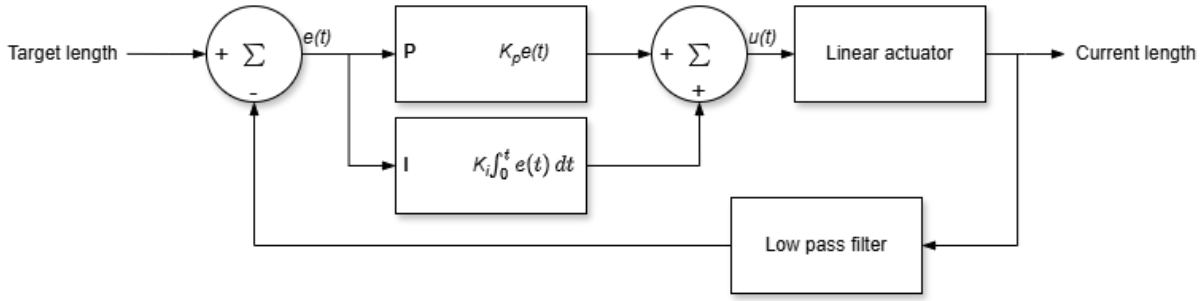

Figure 8: Position PI controller for the linear actuators.

2.4 Data acquisition and processing

Subjects. Two healthy adult volunteers (author and project supervisor) participated in this pilot recording. Owing to time constraints and the exploratory nature of the study, no additional subjects were recruited. Informed consent was obtained from both participants.

Motion-capture acquisition. Mandibular motion was recorded with a five-camera OptiTrack system sampling at 120 Hz. Four reflective markers arranged in a square were attached to the forehead and served as a head-fixed reference frame. A second set of three markers forming a triangle was placed on the gnathion. Two additional lip markers were recorded but later discarded because a single marker cannot encode orientation. [10, 11]

The subject then performed the motion sequences listed in Table 4. Each frame was saved by Motive as a `.csv` file that contains the 3-D marker positions (in millimetres) and the orientation of each marker set as quaternions. The calibrated volume had a residual error of 0.3 mm.

Food	Motion	*Optional:* Duration
Empty mouth	20× open–close cycles	—
Chewing gum (Xylit-Pro, *Excitemint*)	Random side chewing	2 min
	Right-side chewing	1 min
	Left-side chewing	1 min
	Front-teeth-only chewing	1 min
Biscuits (Bretzeli, *Kambli*)	random chewing	—
	front-teeth chew → right-side chew	—
	front-teeth chew → left-side chew	—
	fast random chewing	—
	slow random chewing	—

Table 4: Recording protocol. *Notes:* For chewing-gum trials the first run began with an unchewed piece and the same gum was kept for all subsequent motions. For biscuit trials each run started with an empty, closed mouth; the subject then placed a biscuit, chewed as instructed, and swallowed.

Data processing. To reduce the noise, we apply a 4th-order butterworth filter to the data. The cutoff frequency is set to 6Hz, as human mastication frequency is around 1Hz to 2Hz . The data is then transformed to the head reference frame using rotation matrices.

3 Results

3.1 Mimicking human jaw motion

- human jaw motion from motion capture
- results of PCA on human jaw motion
- show graphs of human jaw motion vs robotic jaw motion
- show graphs of the force during chewing for human vs robot

3.2 chewing force

- max force that can be applied by the robot (both vertical and shear)

4 Discussion

4.1 Summary of findings

4.2 Limitations

- So far very big and heavy robot due to steel plates and big actuator $\neq$ human jaw
- 3D printed teeth/jaw not strong enough to withstand the forces applied by the actuators

4.3 Future work

- 3D printed jaw/teeth to be replaced by a more rigid material
- add a tongue module
- add a saliva module
- adapt state machine to coordinate the different modules
- add a camera to track the food

5 Conclusion

6 References

[1] K Alemzadeh and D Raabe. "Prototyping artificial jaws for the Bristol Dento-Munch Robo-Simulator; 'A parallel robot to test dental components and materials". English. In: (2007). ISBN: 9781424407873 Name and Venue of Conference: 29th Annual International Conference of the IEEE Engineering in Medicine and Biology Society - Lyon, France Conference Organiser: IEEE, EMBS, SFGBM, pp. 1453–1456. DOI: 10.1109/IEMBS.2007.4352574.

[2] Seung-Ju Lee et al. "Design of mastication robot with life-sized linear actuator of human muscle and load cells for measuring force distribution on teeth". In: *Mechatronics* 51 (2018), pp. 127–136. ISSN: 0957-4158. DOI: https://doi.org/10.1016/j.mechatronics.2017.11.013. URL: https://www.sciencedirect.com/science/article/pii/S0957415817301769.

[3] Kazem Alemzadeh et al. "Development of a Chewing Robot with Built-in Humanoid Jaws to Simulate Mastication to Quantify Robotic Agents Release from Chewing Gums Compared to Human Participants". English. In: *IEEE Transactions on Biomedical Engineering* 68.2 (Feb. 2021), pp. 492–504. ISSN: 0018-9294. DOI: 10.1109/TBME.2020.3005863.

[4] Johannes H. Koolstra. "Dynamics of the Human Masticatory System". In: *Critical Reviews in Oral Biology & Medicine* 13.4 (2002), pp. 366–376. ISSN: 1045-4411. DOI: 10.1177/154411130201300406. URL: https://doi.org/10.1177/154411130201300406.

[5] K.C. Julien et al. "Normal masticatory performance in young adults and children". In: *Archives of Oral Biology* 41.1 (1996), pp. 69–75. ISSN: 0003-9969. DOI: https://doi.org/10.1016/0003-9969(95)00098-4. URL: https://www.sciencedirect.com/science/article/pii/0003996995000984.

[6] Charles H. Gibbs et al. "Maximum clenching force of patients with moderate loss of posterior tooth support: A pilot study". In: *The Journal of Prosthetic Dentistry* 88.5 (2002), pp. 498–502. ISSN: 0022-3913. DOI: https://doi.org/10.1067/mpr.2002.129062. URL: https://www.sciencedirect.com/science/article/pii/S0022391302002585.

[7] Sarah C. Woodford et al. "Muscle and joint mechanics during maximum force biting following total temporomandibular joint replacement surgery". In: *Biomechanics and Modeling in Mechanobiology* 23.3 (2024), pp. 809–823. ISSN: 1617-7959. DOI: 10.1007/s10237-023-01807-1. URL: https://doi.org/10.1007/s10237-023-01807-1.

[8] Vassil Svechtarov et al. "Mandibular range of motion and its relation to temporomandibular disorders". In: *Scripta Scientifica Medicinae Dentalis* 1.1 (2015).

[9] Oren Masory and Jian Wang and. "Workspace evaluation of Stewart platforms". In: *Advanced Robotics* 9.4 (1994), pp. 443–461. DOI: 10.1163/156855395X00508. eprint: https://doi.org/10.1163/156855395X00508. URL: https://doi.org/10.1163/156855395X00508.

[10] Steven Mills et al. "Principal Component Representations of Chewing Motion". In: IVCNZ '14 (2014), pp. 218–223. DOI: 10.1145/2683405.2683434. URL: https://doi.org/10.1145/2683405.2683434.

[11] Meg Simione et al. "Differing structural properties of foods affect the development of mandibular control and muscle coordination in infants and young children". In: *Physiology & Behavior* 186 (2018), pp. 62–72. ISSN: 0031-9384. DOI: https://doi.org/10.1016/j.physbeh.2018.01.009. URL: https://www.sciencedirect.com/science/article/pii/S0031938418300155.